Traffic 2009; **10:** 411–424
Blackwell Munksgaard

doi: 10.1111/j.1600-0854.2009.00879.x

A Novel Strategy for the Invasive Toxin: Hijacking Exosome-Mediated Intercellular Trafficking

Fan Zhang†, Shan Sun†, Du Feng†, Wen-Long Zhao and Sen-Fang Sui*

Department of Biological Sciences and Biotechnology, State Key Laboratory of Biomembrane and Membrane Biotechnology, Tsinghua University, Beijing 100084, China
**Corresponding author: Sen-Fang Sui, suisf@mail.tsinghua.edu.cn*
†*These authors contributed equally to this work.*

Toxins penetrate mammalian cells through various means. In this study, we report a unique strategy used by trichosanthin (TCS), a plant toxin with ribosome-inactivating activity, to penetrate host cells. We found that in both JAR and K562 cells, endocytosed TCS is incorporated into intraluminal vesicles of the multivesicular body (MVB) and is then secreted in association with these vesicles upon fusion of the MVB with the plasma membrane. The secreted TCS-loaded vesicles secreted by K562 cells move throughout the intercellular space and target syngeneic and specific allogeneic cells. Subsequent internalization permits delivery of the toxin into the cytosol, resulting in ribosomal inactivation and cell death. Thus, our findings provide a novel mechanism by which foreign proteins pass between and penetrate into mammalian cells.

Key words: cell penetration, exosome, multivesicular body, plant toxin, ribosome-inactivating protein

Received 20 January 2008, revised and accepted for publication 10 January 2009, uncorrected manuscript published online 24 January 2009

A number of plant and bacterial toxins exhibit enzymatic activity toward essential cytosolic constituents, such as elongation factor, ribosomes and actin (1). To gain access to their targets, these toxins must penetrate the cytosol of the host cell after endocytosis. Cytosol translocation is achieved through various means. Endocytosed diphtheria toxin (DT) inserts itself into and penetrates the endosomal membrane by stimulation of acidic endosomal pH (2). Ricin and shiga toxins target retrograde transport along the secretory pathway, by which they are delivered into the endoplasmic reticulum through the Golgi apparatus, and then finally enter the cytosol through the Sec61 complex (3). However, the method of translocation remains unknown for certain clinically significant toxins, such as trichosanthin (TCS).

TCS is a plant toxin isolated from the root tuber of *Trichosanthes kirilowii*. It consists of a 27-kD polypeptide chain with high similarity to the ricin A chain (4,5). TCS also exhibits intrinsic RNA *N*-glycosidase activity, through which it removes an important adenine from 28 *S* ribosomal RNA, resulting in the inactivation of eukaryotic ribosomes (6). TCS preferentially targets syncytiotrophoblast cells, malignant cells and macrophages, for which reasons it has been exploited clinically as an abortifacient, as an antitumor agent and in immunomodulation (7–9). In addition, TCS has also been identified as a potential anti-acquired immune-deficiency syndrome drug because of its unique ability to inhibit the replication of HIV-1 in both T cells and monocyte-derived macrophages (10,11).

TCS is internalized by host cells through clathrin-coated vesicles, followed by ribosome inactivation and cell death (12,13). However, the translocation pathway of TCS is poorly understood. In this study, we present evidence indicating that in JAR and K562 cells, two general host cells of TCS, endocytosed TCS is incorporated into and transported along a unique intercellular trafficking pathway mediated by exosome-like vesicles (ELV).

Results

Endocytosed TCS is released from cells in association with ELV

The dynamic transport of fluorescein isothiocyanate (FITC)-labeled TCS, which acts in the same manner as the native toxin as reflected by the toxicity curves (Figure S1), was examined in JAR and K562 cells. In both cell lines, some TCS molecules were quickly internalized into small peripheral vesicles within 10 min and then delivered into larger vacuolar compartments about 30 min later. After further incubation, toxin molecules were detected in unique pomegranate-like organelles. Prolonged incubation led to further concentration in small vesicle-like structures, giving the appearance of clusters of bright dots. About 150 min after endocytosis, a number of TCS-stained dots were observed at the cell surface, followed by apparent exportation from the cell (Figure S2).

To determine whether TCS was secreted from cells, culture supernatants collected from FITC-TCS-treated K562 cells were subjected to immunoblotting. As shown in Figure 1A, endocytosed TCS was detected in supernatants collected from TCS-treated K562 cells after 90–120 min of chase incubation. Moreover, sucrose density flotation analysis indicated that secreted TCS exhibited a markedly lower buoyant density (range, 1.1–1.2 g/mL; Figure 1B, upper panel) than free TCS (Figure 1B, lower

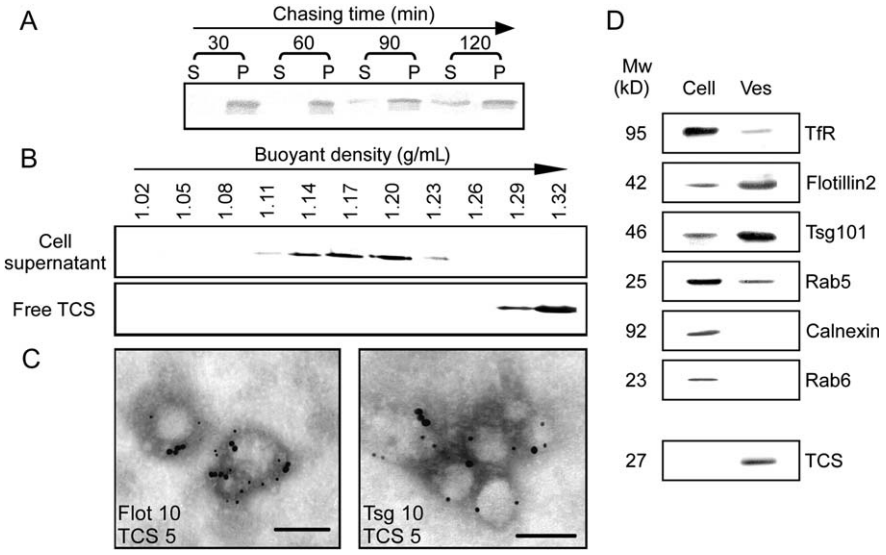

Figure 1: TCS is released from cells in association with ELV. A) Immunoblotting analysis of TCS in cell pellets and cell culture medium. K562 cells were pulsed with 0.2 μM TCS for 30 min and then chased with TCS-free medium for 30–120 min. The culture mixture was centrifuged at 300 × ***g*** for 10 min to produce a cell pellet (P). The supernatant (S) was passed through a 0.22-μm filter to remove cellular debris, concentrated through Centriprep filtration and then subjected to immunoblotting. B) Continuous sucrose density flotation analysis of cell culture supernatants. Culture supernatants collected from K562 cells after treatment (30-min pulse and 120-min chase) with TCS (upper panel) or 0.05 μM TCS dissolved in cell-free medium (lower panel) were centrifuged on a 0.25–2.5 M continuous sucrose density gradient. C and D) IEM of isolated vesicles. Samples were immunogold labeled for TCS (5 nm) and flotillin2 (10 nm) or for TCS and tsg101 (10 nm). Scale bar, 100 nm.

panel), further confirming that these toxins were secreted from cells in association with a lipid membrane rather than as a 'naked' protein.

To further characterize this TCS-containing fraction, the cell culture medium was subjected to differential centrifugation. Following final centrifugation at 100 000 × ***g***, pellets were analyzed by immunoelectron microscopy (IEM), which revealed the presence of small, TCS-rich membrane vesicles with an average diameter of 50–100 nm (Figure 1C,D). The size and morphology of these vesicles were reminiscent of 50- to 90-nm vesicles of endosomal origin, known as exosomes, that are released by many cell types (14). To determine whether the TCS-containing vesicles exhibited other exosome-like characteristics, cell lysates and vesicles were then tested for the presence of proteins known to be enriched in exosomes (Figure 1D). In addition to loading significant amounts of TCS, the purified vesicles were also enriched in flotillin2 and Tsg101 (Figure 1D), important exosomal components in several cell types (15–18). The presence of flotillin2 and Tsg101 was also confirmed by IEM (Figure 1C,D). Furthermore, the transferrin receptor (TfR) and rab5 were detected in TCS-positive vesicles, although their contents were lower than in the cell lysate. As a control, neither rab6 nor calnexin was detected in purified membrane, excluding the possibility of contamination of the isolated exosomes with cell debris (Figure 1D). Taken together, these observations indicate that TCS released by cells was associated with exosome-like membrane vesicles.

TCS-containing vesicles originate from the multivesicular body

Exosomes correspond to the internal vesicles of the endosomal compartment, the multivesicular body (MVB) (19). To ascertain the intracellular origin of TCS-containing vesicles, we examined the molecular and morphological features of TCS-targeted organelles. JAR cells pretreated with FITC-TCS were immunoprobed with various molecular markers. Confocal fluorescence microscopy showed clear colocalization of endocytosed TCS and Lamp1, LBPA and rab7, a group of proteins known to be targeted to the MVB (15,20–22) (Figure 2A). Electron microscopy was used to resolve the ultrastructure of TCS-targeted organelles. In agreement with previous studies demonstrating that TCS enters the MVB (13), endocytosed TCS was detected in large multivesicular compartments composing a limiting membrane that enclosed a number of 30- to 100-nm intraluminal vesicles in both JAR and K562 cells (Figure 2B,E). Moreover, TCS molecules were targeted to the intraluminal vesicles of the MVB in association with the membrane protein flotillin2, indicating that TCS was not freely dissolved within the lumen of these organelles (Figure 2C,E). We also obtained evidence for the exocytosis of MVBs. In both JAR and K562 cells, we observed the TCS-targeted MVB fusing with the plasma membrane at the cell surface, where a number of TCS-associated vesicles accumulated and were released into the extracellular medium (Figure 2D,F). However, it could also be the profile of exosome re-entry as described in the following experiment.

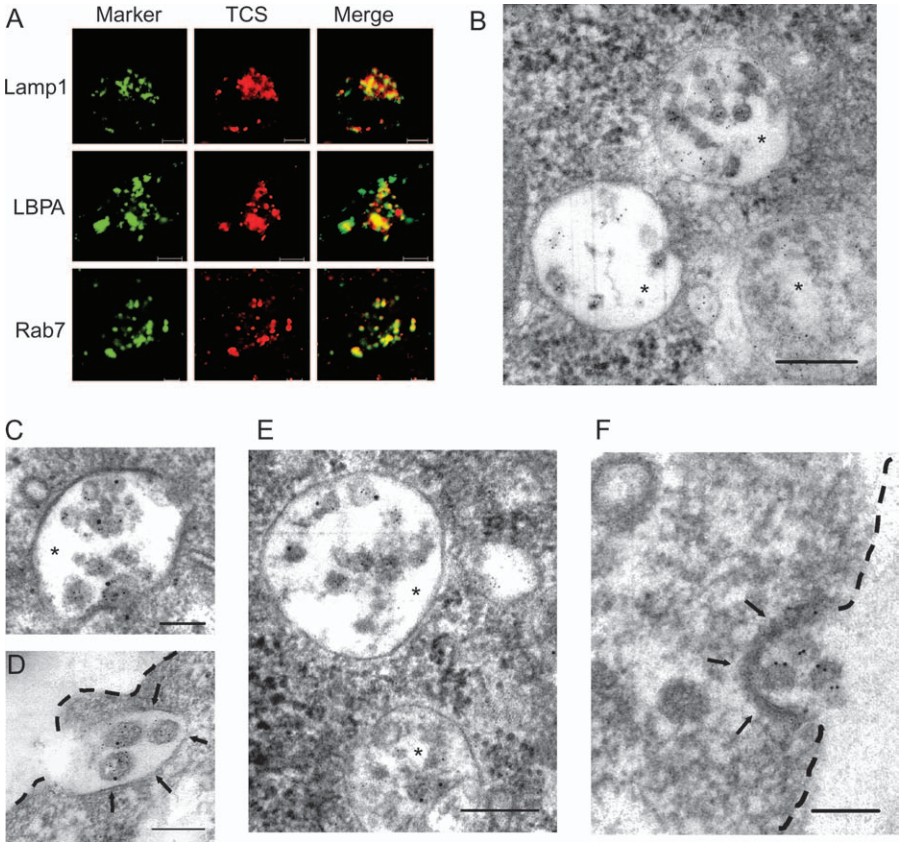

Figure 2: TCS localizes to the MVB. A) Laser scanning confocal microscopy of TCS-targeted organelles. JAR cells were pulsed with FITC-TCS for 2 h and then chased with TCS-free medium for 2 h, followed by immunolabeling for Lamp1, LBPA or rab7. Fluorescence images for immunoprobed markers (green), for FITC-TCS (red) and merged images are shown. Scale bar, 20 μm. B–F) Electron microscopy of TCS-targeted MVB and exocytosis. JAR cells (B–D) or K562 cells (E and F) were pulsed with TCS for 30 min and then chased with TCS-free medium for 60 min (B, C and E) or 120 min (D and F). Ultrathin sections were immunogold labeled for TCS (5 nm; B and F) or for both TCS (5 nm) and flotillin2 (10 nm) (C–E). Asterisks in B, C and E indicate the TCS-targeted MVB. Dashed lines in D and F indicate the profile of the cell surface. Arrows indicate the TCS-targeted MVB fusing with the plasma membrane. Scale bar, 200 nm in B and E; 100 nm in C, D and F.

Taken together, these results indicate that endocytosed TCS is incorporated into MVB intraluminal vesicles and then secreted from cells in ELV, forming TCS-loaded vesicles secreted by K562 cells (TLVs). Supporting this finding, such vesicle-associated secretion of TCS was stimulated by treating cells with monensin, a drug known to enhance exosome production by stimulating MVB exocytosis (23,24), but inhibited by treatment with wortmannin, a drug known to impair MVB formation by inactivating phosphatidylinositol 3-kinase (25,26), and thus inhibits exosome formation. Consistently, using small RNA interfering with Tsg101 (the level of knockdown was ~80% of control; Figure S3A), a component of endosomal complexes required for transport-I (ESCRT-I) that functions in the early stage of MVB formation (27), resulted in 40% decreased production of either normal exosomes or TLVs. It is recently reported that ceramide, a lipid produced from the membrane lipid sphingomyelin by sphingomyelinases (SMases), triggers budding of exosome vesicles (28). To address the specificity of exosome pathway, we decreased the amount of ceramide by disrupting the expression of neutral sphingomyelinase 2 (nSMase2) with the use of specific inhibitor, GW4869, or RNA interference (RNAi) of nSMase2 (the nSMase2 RNA level of knockdown was ~92% of control; Figure S3B). The results proved that the productions of both total exosomes and TLVs were consistently decreased markedly in treated cells compared with control cells, showing a strong correlation of TLV production with exosome biogenesis (Figure 3).

TCS is targeted to both the membrane and the lumen of ELV

Next, we examined the distribution of TCS in TLVs. Purified TLVs were permeated with 0.1% Triton-X-100 and then centrifuged. Immunoblotting revealed that most vesicle-associated TCS was deposited in pellets, together with the membrane proteins TfR and flotillin2, indicating that toxin molecules were membrane associated (Figure 4 A). However, a small amount of toxin was detected in the supernatant after permeation, which may reflect release from the membrane or from the lumen of these vesicles.

To clarify this point, we treated TLVs with trypsin or pronase, assuming that toxin molecules enclosed within the TLV lumen would be protected from hydrolysis. As expected, both trypsin and pronase quickly degraded most TLV-associated TCS within 15 min, while some intact toxin persisted after 1 h of digestion and could only be destroyed after permeating the TLV membrane with Triton-X-100 (Figure 4B, upper panel). As controls, TCS dissolved in phosphate buffer showed complete degradation within 15 min in the presence or absence of detergent (Figure 4B, lower panel). These results clearly indicate that TCS is distributed within the membrane and the lumen of TLVs.

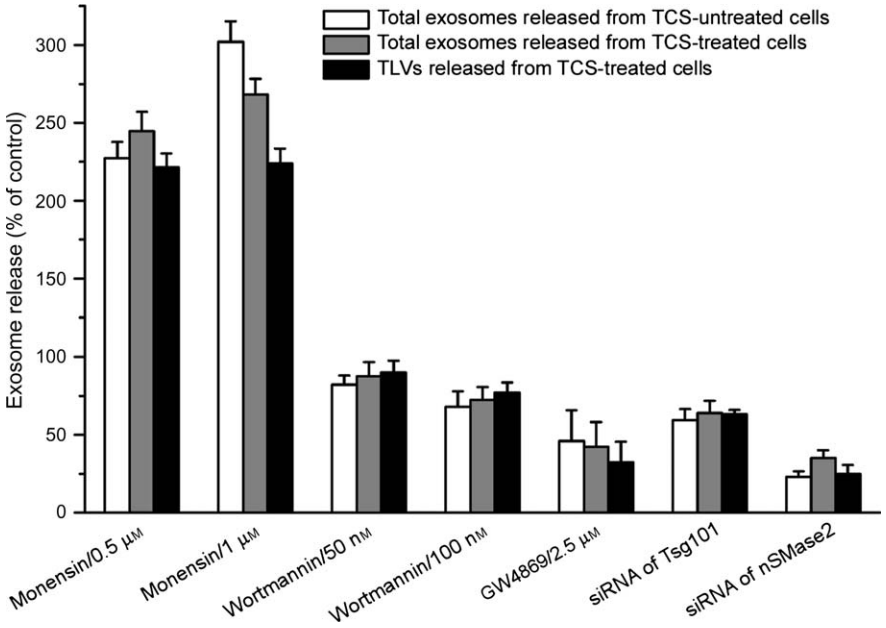

Figure 3: Effects of various treatments on the secretion of TLVs. The secretion of total exosomes or TLVs over a 24-h period was quantified in untreated K562 cells (control) or K562 cells grown in medium containing the indicated concentrations of wortmannin, monensin or GW4869. For tsg101 RNAi analysis, K562 cells were transfected with the plasmid pBS/U6/T (siRNA for tsg101) or pBS/U6/NC (control). For nSMase2 RNAi analysis, an siRNA targeting human nSMase2 (siRNA for nSMase2) or scrambled siRNA (control) was delivered into K562 cells. All data were normalized by dividing against the total number of viable cells after 24 h as determined by the MTT method. The indicated values represent the mean ± SEM of three independent experiments.

Specific interaction with lipid rafts contributes to the exosomal incorporation of TCS

Although TCS is a soluble protein, the preceding experiments demonstrate that TCS is tightly associated with TLVs and is able to penetrate the membrane. To understand how TCS interacts with the membrane, we examined its distribution within the TLV membrane.

The membrane portion of TLVs was isolated by permeation with 0.1% Triton-X-100 as described above (Figure 4A) and then treated with different concentrations of detergents to separate the microdomains. The supernatant and the detergent-resistant membrane pellet obtained from centrifugation were submitted to SDS–PAGE and analyzed by western blotting for TCS. The results revealed that all the exosome membrane-associated TCS was in the microdomains that were resistant to 0.5 and 1% Triton-X-100 as well as 1% 3-[(3-cholamidopropyl)-dimethylammonio]-1-propane sulfonate (CHAPS) (Figure 5A, upper panel), findings reminiscent of the definition of raft-like microdomains. Flotillin2, a representative raft-associated protein, was also detected in the TCS-positive detergent-resistant membrane pellets (Figure 5A, middle panel). In contrast, the TfR that is usually excluded from rafts was almost all dissolved in the supernatant after detergent treatment (Figure 5A, lower panel).

We then subjected Triton-treated TLV mixtures to sucrose density flotation. Although TfR remained at the bottom of the sucrose gradient after centrifugation (Figure 5B, lower panel), both TCS and flotillin2 moved into the lower fractions (Figure 5B, upper and middle panels). These results are consistent with the features of raft-like microdomain-associated proteins. Furthermore, when we treated TLVs with 5 mM methyl-β-cyclodextrin (MBCD) and/or 0.5 units SMase to remove two important components of lipid rafts, namely cholesterol and sphingomyelin, respectively, the detergent resistance of both TCS and flotillin2 in TLV membranes decreased markedly (Figure 5C).

These results consistently demonstrate that TCS is targeted to raft-like microdomains in the TLV membrane.

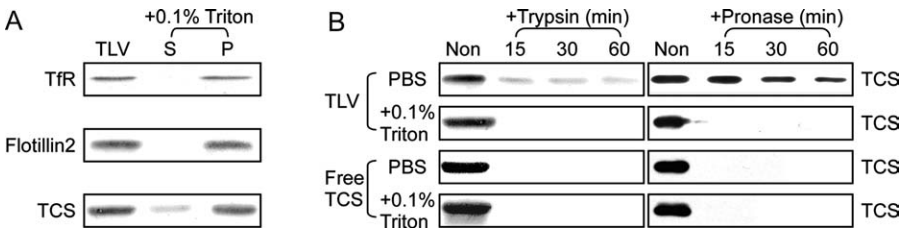

Figure 4: TCS is targeted to both the membrane and the lumen of secreted ELV. A) Purified TLVs were treated with PBS containing 0.1% Triton-X-100 for 30 min at room temperature and then centrifuged. Equivalent amounts of untreated TLVs, permeated supernatant (S) and membrane pellet (P) were analyzed by immunoblotting. B) TLVs or free TCS were digested with 1 mg/mL trypsin or pronase in PBS or PBS containing 0.1% Triton-X-100 at 37°C for the indicated times. After digestion, reaction mixtures were concentrated by Centriprep filtration and analyzed by immunoblotting.

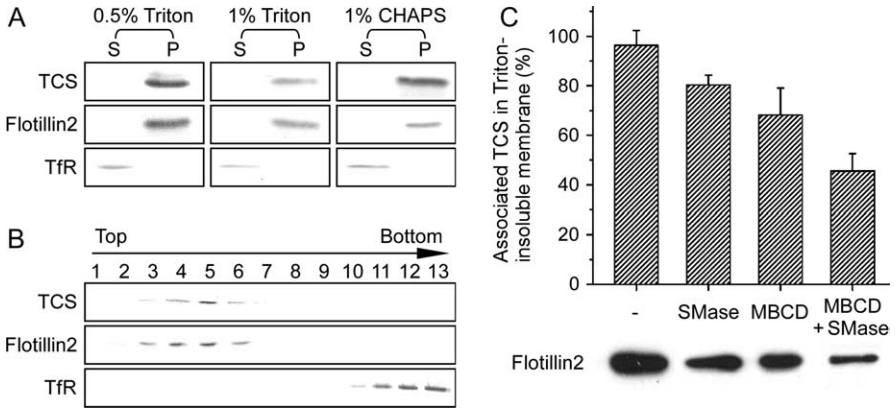

Figure 5: TCS is specifically targeted to raft microdomains on the exosomal membrane. A) Detergent solubilization of TLV membrane. TLV membrane was isolated and then treated with 0.5% Triton-X-100, 1% Triton-X-100 or 1% CHAPS at 4°C overnight. The detergent-soluble (S) and detergent-resistant fractions (P) were separated by centrifugation and analyzed by immunoblotting. B) Sucrose density flotation. 1% Triton-treated TLV membrane mixture was loaded onto a discrete gradient of 40, 30 and 5% sucrose for centrifugation at 270 000 × ***g*** for 18 h. After centrifugation, 13 fractions were collected from the top of the column and then analyzed by immunoblotting. C) Raft depletion analyses. FITC-TCS-rich TLVs were treated with MBCD and/or SMase at 37°C for 6 h and then solubilized with 1% Triton-X-100. The detergent-resistant membrane fraction was pelleted by centrifugation and then analyzed by immunoblotting for flotillin2 (lower panel) or by fluorescence spectroscopy (at 495-nm excitation) to quantify the associated FITC-TCS (upper panel). The fluorescence intensity of TCS in Triton-resistant membrane from untreated TLVs (-) was defined as 100% (the original value was 358).

Recent evidence indicates that lipid rafts are concentrated within MVB intraluminal vesicles or secreted exosomes (29–31), which contributes to the sorting of a number of raft-associated membrane proteins, including flotillin2, glycosyl-phosphatidylinositol anchor proteins and tetraspanins (16,27). Therefore, we examined whether lipid rafts play an important role in the incorporation of endocytosed TCS into exosomes.

First, we examined the interaction between TCS and purified exosomes, the equivalent of MVB intraluminal vesicles, under conditions mimicking the interior of the MVB. After incubation with TCS for 4 h at 37°C in pH 5.0 culture medium, the exosomes were pelleted by centrifugation and analyzed by western blotting. Although TCS at the lower concentrations (0.1–0.2 μM) showed quite a weak interaction with the exosomes, a significant amount of toxin was recruited into these vesicles after TCS was concentrated 5–10 times in the bulk phase (Figure 6A), and its distribution was very similar to that of cell-derived TLVs, that is, both in the membrane and in the lumen (Figure 6B,C). However, such targeting of TCS was highly dependent on the presence of lipid rafts in the exosome membrane; pretreatment of exosomes with MBCD and/or SMase, which destroy lipid rafts, greatly decreased the amount of exosome-associated TCS (Figure 6D).

These results were further confirmed by additional liposome analyses. When TCS was incubated with vesicles prepared from different lipid mixtures, the toxin was specifically targeted to liposomes with exosome-like or raft-like composition but not to liposomes containing only neutral phospholipids [i.e. phosphatidylcholine (PC) and phosphatidylethanolamine (PE); Figure 6E]. Furthermore, combined analyses of detergent treatment and trypsin hydrolysis revealed that TCS was tightly associated with the membrane and penetrated into the lumen of both exosome-like and raft-like liposomes (Figure 6F,G), which is similar to the distribution of TCS in exosomes. These results strongly suggest that interaction with lipid rafts is sufficient to incorporate TCS into artificial liposomes or exosomes.

Finally, the molecular basis of this specific interaction between TCS and lipid rafts was investigated. Membrane biophysical analyses revealed that TCS penetrated the raft-like monolayer more effectively than the neutral phospholipid (PC/PE) monolayer as was reflected by the critical insertion pressure (Figure S4). Furthermore, the presence of lipid rafts increased membrane insertion, even reaching the hydrophobic core of the lipid bilayer (Figure S5), which may provide an opportunity for TCS to further penetrate into the lumen of exosomes or liposomes. However, the details of this process require further investigation (see detailed results in Supplementary Materials and Methods).

Intercellular trafficking of TLV and cytosol delivery of TCS

Exosomes are thought to participate in intercellular membrane trafficking (19,32). Therefore, we examined whether TLVs are involved in a similar process. First, two groups of cells were pretreated with either FITC-TCS or tetramethylrhodamine isothiocyanate (TRITC)-TCS and then co-

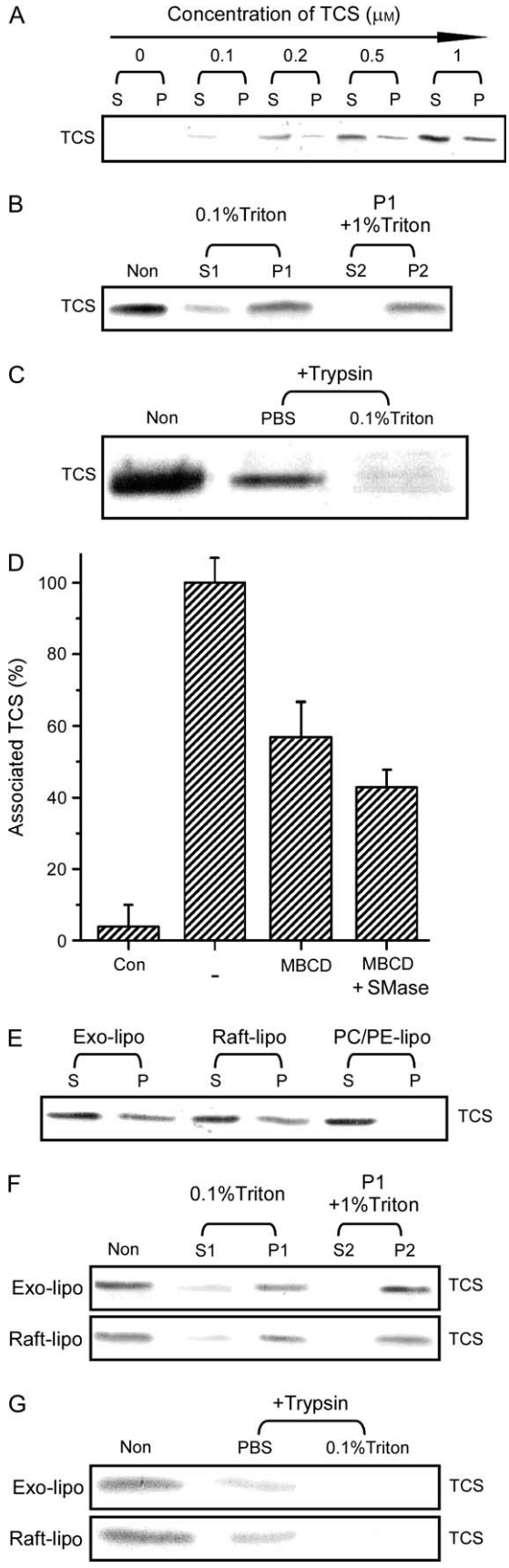

Figure 6: Interaction with lipid rafts contributes to exosomal targeting of TCS. A) TCS targeting to the purified exosomes *in vitro*. Purified K562-derived exosomes were incubated for 4 h at 37°C and pH 5.0 at the indicated concentrations of TCS in RPMI-1640 medium (containing 10 mM HEPES and 50 mM NaAc). After centrifugation, the pellet was washed and subjected to immunoblotting. B and C) Distribution of TCS in reconstituted TLV (rTLV). B) rTLVs prepared by incubating exosomes with 1 μM TCS were treated with 0.1 and 1% Triton-X-100 in sequence. Intact rTLV and sequential fractions of detergent treatments were analyzed by immunoblotting. C) rTLVs were digested with 1 mg/mL trypsin in PBS or PBS containing 0.1% Triton-X-100 at 37°C for 1 h. After digestion, reaction mixtures were concentrated by Centriprep filtration and analyzed by immunoblotting. D) Effects of raft depletion on exosomal targeting of TCS. Purified exosomes were treated with MBCD alone or MBCD and SMase at 37°C for 6 h and then incubated with 1 μM FITC-TCS for an additional 4 h. After centrifugation, the exosomes were washed in a large volume of PBS and then analyzed by fluorescence spectroscopy (at 495-nm excitation) to quantify TCS incorporation. The fluorescence intensity of TCS in untreated exosomes (-) was defined as 100% (the original value was 741). Con, exosomes without FITC-TCS treatment. E) Selective interaction of TCS with raft-containing liposomes. Liposomes (200 μM) with a composition similar to that of exosomes (exo-lipo), lipid rafts (raft-lipo) or liposomes composed only of neutral phospholipids (PC/PE-lipo) were incubated with 1 μM TCS at 37°C in pH 5.0 acetate buffer (containing 100 mM NaCl) for 4 h and then pelleted, washed and subjected to immunoblotting. F and G) Distribution of TCS in liposomes. Exo-liposomes or raft-liposomes were incubated with 1 μM TCS as described above. After centrifugation, liposome pellets were subjected to Triton solubilization (F) or trypsin hydrolysis (G) as described in (B and C). S, supernatant; P, pellet.

incubated. After a period, a large number of fluorescent TLVs were secreted and targeted to cell surface. In particular, some cells collected both FITC-tagged and TRITC-tagged vesicles, indicating that secreted TLVs are transferred between neighboring cells (Figure 7A, left and middle panels). Interestingly, intercellular TLV trafficking also occurred between allogeneic JAR and K562 cells (Figure 7A, right panel). Moreover, TLVs targeted to Jurkat cells and NK92 cells (Figure S6), whereas neither 293T nor sp2/0 cells accepted TLVs (data not shown), suggesting a limited selectivity of TLVs for target cells.

To determine the fate of TLVs in target cells, we incubated purified FITC-labeled TLV with untreated JAR or K562 cells. Fluorescence microscopy showed that these vesicles were targeted to the cell surface within 30 min and then internalized and delivered into intracellular regions near the nucleus within 60 min (Figure 7B). Similarly, electron microscopy revealed that upon reaching the cell surface, TLVs were trapped in endocytic pits in the plasma membrane and then internalized into large perinuclear organelles (Figure 7C,D).

Because TLVs are endocytosed by target cells, we examined whether these TCS-rich vesicles were capable of inactivating ribosomes to inhibit protein synthesis and further inducing cell death. The protein synthesis was

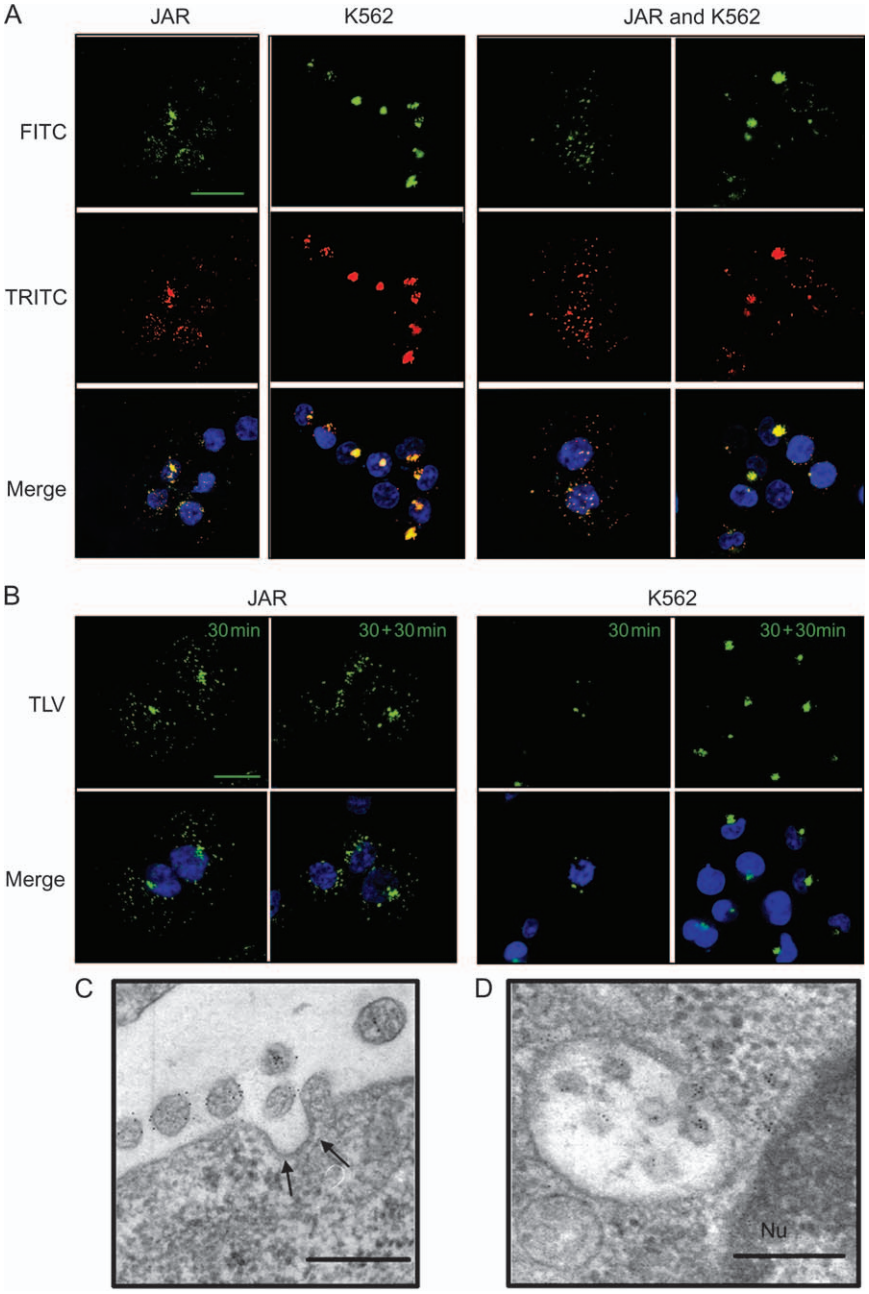

Figure 7: Intercellular trafficking and uptake of TLVs. A) Intercellular trafficking of TLV in JAR cells (left), K562 cells (middle) or among JAR and K562 cells (right). Two groups of cells were pretreated with FITC-TCS (green) or TRITC-TCS (red) as described in the *Materials and Methods* and then mixed and co-incubated for 120 min. To track TLV trafficking between JAR and K562 cells, JAR cells were pretreated with FITC-TCS and K562 cells with TRITC-TCS. Blue, nuclear staining using 4′-6-diamidino-2-phenylindole (DAPI). Scale bar, 20 μm. B) Dynamic transport of TLV in target cells. JAR (left) or K562 cells (right) were incubated with purified FITC-labeled TLV for 30 min or pulsed for 30 min and then chased for 30 min. Blue, DAPI staining. Scale bar, 20 μm. C and D) Electron microscopy of K562 cells that were incubated with purified TLV for 10 min (C) or pulsed for 10 min and then chased for 60 min (D). Arrows in (C) indicate the endocytic pits targeted by TLVs. Nu, nucleus. Scale bar, 200 nm.

measured using the [^{3}H]leucine incorporation assay. In K562 and JAR cells, TLVs containing 70 ng of TCS exhibited the higher inhibitory effect on the leucine incorporation than the same amount of naked TCS, while normal exosomes secreted by K562 cells (NE) had no visible effect on these cells (Figure 8). These results were consistent with those from cytotoxicity assays in K562, JAR, Jurkat and NK92 cells using 3-(4,5-dimethylthiazol-2-

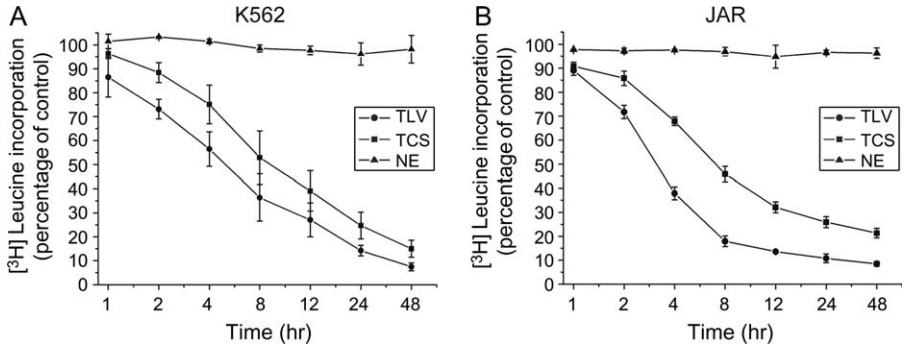

Figure 8: Protein synthesis inhibition assay. A) K562 and (B) JAR cells were incubated with 70 ng of naked TCS, TLVs containing 70 ng of TCS or the same amount of NE for the indicated times. Then, cells were treated with 1 μCi of [^{3}H]leucine for 20 min. The incorporated radioactivity was determined by liquid scintillation counting. The results are expressed as the percentage of the leucine incorporation in the untreated control cells and indicated as mean ± SEM from three separate experiments.

yl)-2,5-diphenyltetrazolium bromide (MTT) method. In all cell types, toxin-rich TLVs elicited more severe toxicity, in a dose-dependent manner, than the naked protein (Figure 9). In contrast, normal K562 exosomes had no visible effect on any cell type. Especially, TCS treatment in Jurkat cells showed no effect after 48 h but TLV treatment did, which may be because that Jurkat cells could accept TCS-loaded exosomes much more efficiently than naked TCS proteins.

Discussion

The experiments described in this study demonstrate a novel translocation pathway for the plant toxin TCS. Instead of the more common pathway of intracellular translocation, our data show that TCS is targeted to MVB-derived small secretory vesicles that penetrate target cells through intercellular vesicle trafficking.

Endocytosed toxins must escape lysosomal degradation to exert their toxic action. They do so by directly penetrating the endocytic compartment, such as DT, or by bypassing intracellular vesicle trafficking, such as ricin and shiga toxins (1). In the present study, however, TCS was released from cells in membrane vesicles, despite the possibility that some of the toxin molecules might have been further degraded. Importantly, we determined that these TCS-rich vesicles exhibited exosome-like features (Figures 1 and 2) (33). Exosomes are small membrane vesicles released by many cell types upon fusion of MVBs with the plasma membrane (14). They mediate the secretion of specific endogenous proteins, such as prions (18), Hsp60 and 70 (34,35) and major histocompatibility complex (MHC) class I and class II (19,33,36), but there have been few such reports regarding exogenous proteins. In this study, we describe an exogenous TCS protein that was exported from cells in association with exosomes. Recent research suggested that T-cell-induced secretion of exosomes from activated B cells allowed antigenic peptide–MHC class II complexes to escape lysosomal degradation in B cells (37). Thus, in the case of the foreign protein TCS, our observations strongly suggest that TCS uses the exosomal pathway to avoid degradation in host cells.

An interesting observation was that an approximately 80% decrease of the expression level of Tsg101 caused only an approximately 35% reduction of the TLVs, which suggested that some exosomes might form independently of Tsg101. It has been reported that Tsg101 depletion caused a small reduction in the number of MVBs in A431 cells, suggesting that Tsg101 is required for MVB formation but that some MVBs may form independently of Tsg101 (38). Because exosomes correspond to the internal vesicles of the MVB, such a finding could also suggest that some Tsg101-independent mechanism might contribute to the formation of exosomes. Moreover, recent researches find that formation of proteolipid protein-containing exosomes in an oligodendrocyte cell line does not require ESCRT machinery and that ceramide, a lipid produced from the membrane lipid sphingomyelin by SMases, triggers budding of exosome vesicles into MVBs, providing an alternative pathway for sorting cargo into MVBs and exosome formation (28,39). Because exosomes originated from different cells and subpopulations of exosomes derived from the same cell differ in their protein and lipid contents (40–42), it is possible that various mechanisms for exosome formation could coexist in cells. Besides, we also found that TCS itself is an activator of exosome biogenesis; at 1 μM, it increased the production of K562-derived exosomes by 50–80%, although the detailed mechanism is unclear (Figure S7).

These results raise a fundamental question regarding the mechanism by which TCS is targeted to exosomes. Exosomes originate from internal vesicles of the endosomal compartment, the MVB (19). Consistent with this, we found that TCS was primarily incorporated into the vesicular region of MVBs (Figure 2). A series of previous

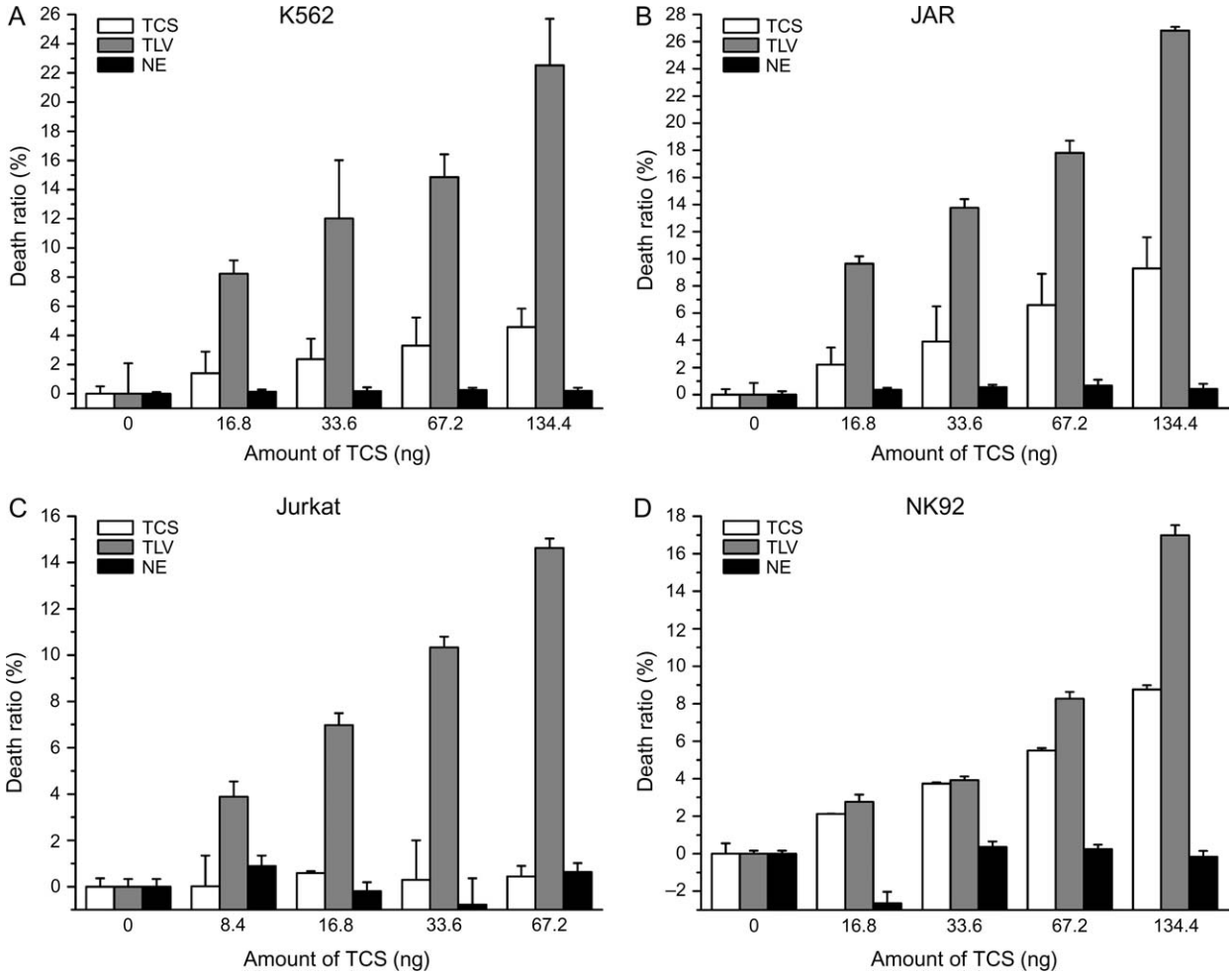

Figure 9: Cytotoxicity of TLV. Cells were incubated with indicated amounts of naked TCS, TLVs containing the indicated amount of TCS or the same amount of NE in growth medium for 48 h at 37°C. Cells grown in the absence of TCS, TLV and NE were used as controls (A)K562,(B)JAR,(C)Jurkat,and (D)NK92 respectively. The death ratio was measured using the MTT method as described in the *Materials and Methods*. The bars indicate the mean ± SEM of three independent experiments.

studies indicated that lipid raft microdomains were enriched in the intraluminal vesicles of the MVB and in exosomes (29–31). It is also notable that TCS is specifically targeted to the raft microdomains of exosomes and that TCS selectively interacts with these domains *in vitro* (Figures 5 and 6). Therefore, it is possible that selective targeting to raft microdomains may provide a sorting drive for exosome incorporation. In fact, a number of other membrane proteins sort selectively into exosomes based on their preference to partition into such microdomains (16,18,43).

In addition, using liposomes mimicking exosomes (exo-liposome), raft microdomains (raft-liposome) and non-raft membrane (PC/PE-liposome), we found that TCS is recruited to exo-liposomes and raft-liposomes, both of which contain raft components, but not to PC/PE-liposomes. These results indicate that TCS interacts selectively with raft microdomains. In addition, detergent treatment and trypsin digestion demonstrated that the distribution of TCS in these two types of liposomes was very similar to that in cell-derived TLVs, with TCS enrichment in the membrane (raft microdomains) and the lumen. These results indicate that interaction with raft microdomains is a primary factor contributing to the incorporation of this toxin into exosomes. Furthermore, additional molecular biophysical analyses showed that TCS can selectively and deeply insert itself into membrane containing raft components, even reaching the hydrophobic core of the lipid bilayer, which may contribute to the penetration of TCS into the lumen of the exosome or liposome, resulting in the observed dual distribution. As previously reported, anthrax toxin can also translocate across the endosomal membrane to reach the lumen of the intraluminal vesicles (44,45). When exposed to acidic pH, the heptamerized protective antigen of anthrax toxin inserts into membranes and forms ion-conductive channels resulting in the translocation of the lethal factor (44,45). This mechanism provides a clue

on how TCS translocates across the membrane. However, further research is required to understand this process in greater detail.

Exosomes are thought to mediate intercellular trafficking (46–49). Our further investigation into the fate of secreted TLVs also supports this role for exosomes. Regardless of whether the vesicles could target their origin cells, the secreted TLVs spread rapidly throughout the extracellular milieu and target other syngeneic cells and certain allogeneic cells through some unknown recognition mechanism (Figure 7). In target cells, TLVs were internalized into large endocytic compartments (Figure 7), likely late endosomes or the MVB, based on their deep intracellular localization and colocalization with Lamp1 (unpublished data). It is possible that MVBs in TLV origin cells and target cells are distinct subpopulations of MVBs, with one population preferentially secreting exosomes and another population enriched in internalized exosomes. Support for this hypothesis comes from data describing the existence of distinct MVB subtypes that share morphological characteristics but differ in terms of protein and lipid compositions (50,51). The internalized TLVs may finally release all or a portion of the toxin into the cytosol of target cells through some unknown molecular mechanism. Because TCS showed a unique dual distribution in the membrane and lumen of TLVs (Figure 4), it is possible that cytosolic delivery of toxin-rich TLVs may be the result of the fusion of these vesicles with late endosomes/lysosomes in their target cells, which would release luminal content directly into the cytosol. Support for this hypothesis comes from data showing that the incorporation of vesicular stomatitis virus-G, a viral fusion protein, into ELV provided enhanced presentation of exosomal antigens by DC; this was the result of ELV internalization into the acidic endolysosomal compartment, from which the antigen gained access to the pathway for MHC class I presentation (51).

Based on our results, we propose a novel translocation pathway for TCS. After endocytosis, TCS is delivered into the MVB and incorporated into the intraluminal vesicles of this organelle. Followed by the fusion of the MVB with the plasma membrane, TCS-associated intraluminal vesicles are released into the extracellular medium, forming TLVs. Within TLVs, TCS is not only associated with the vesicle membrane but also found in the lumen. The secreted TLVs then spread throughout the intercellular space and are targeted to syngeneic cells or specific allogeneic cells. After internalization, TCS is released into the cytosol. Thus, by hijacking this exosome-mediated intercellular trafficking pathway, TCS not only escapes intracellular degradation but also gains access to the cytosol, where it may then exert its toxic effect. This hypothesis is supported by the fact that exosome-mediated TCS elicits more severe toxicity than the naked protein, which may reflect trafficking benefits in terms of more efficient internalization and targeting. Therefore, we would like to propose the exosome-mediated transport of TCS as a main pathway of intoxication. Further *in vivo* studies are required to examine this hypothesis. Nonetheless, we did not exclude the possibility that TCS may have other translocation bypass, such as directly penetrating the endocytic compartment induced by acidic pH. Although the transport pathway of TCS we proposed is similar to anthrax toxin to some extent in the intracellular pathway, the mechanism of TCS action is different (44). The TCS toxin-containing vesicles can be secreted to extracellular medium, forming TLVs, which would be further internalized by cells and finally release the loaded TCS into the cytosol.

As indicated by recent evidence, mammalian cells secrete exosomes not only *in vitro* but also *in vivo*, in human blood, urine and tissue effusions (52–54). Thus, exosomes may provide a natural vehicle for molecules to survive in the body and transmit themselves between different tissues. Our results indicate that TCS uses this pathway by forming a unique toxin-loaded vesicle. There is a well coincidence of the pharmacological property of TCS in antitumor and immune regulation (7,9,55) with the effect of TLV on some tumor and immune cells as indicated in this work, which may provide insight into its pharmacological properties in antitumor and immune regulation (7,9,55). Thus, our results regarding the exosome-mediated translocation of TCS may provide important information for future medical research and further applications for TCS and exosomes.

Materials and Methods

Cell, reagents and antibodies

Fluorophores and chemical reagents were purchased from Sigma. Antibodies for TfR (CD71), flotillin2, rab5, rab6, calnexin and Tsg101 were purchased from Santa Cruz Biotechnology. Rabbit anti-TCS poly-antibody was prepared as standard protocol. Horseradish peroxidase-labeled and fluorescently labeled secondary antibodies were purchased from Zhong Shan Biotechnology. Ten-nanometer gold-labeled protein A and 5-nm gold-labeled secondary antibody were purchased from Sigma and Jackson ImmunoResearch, respectively. JAR (human choriocarcinoma) and K562 (human erythroleukemia) cells were purchased from the Institute of Biochemistry and Cell Biology of the Chinese Academy of Sciences. TCS was purified from the root tubers of *T. kirilowii* (Tianhuafen) as previously described by Xia and Sui (56).

Differential centrifugation and exosome/TLV isolation and quantification

NE or TLVs were isolated from the 24-h culture supernatant of K562 cells grown in the complete medium without or with 0.2 μM TCS (FITC-TCS) by differential centrifugations as described by Raposo et al. (21). Briefly, the collected culture mixture was centrifuged at 300 $\times$ ***g*** for 10 min, 800 $\times$ ***g*** twice for 15 min and 10 000 $\times$ ***g*** for 30 min to remove cells and debris. The supernatant was further filtered by a 0.22-μm filter, ultrafiltrated and condensed through Amicon Ultra-15. To eliminate molecules smaller than 100 kD, we washed the Amicon Ultra-15 tube for five times using PBS and centrifuged at 100 000 $\times$ ***g*** for 2 h to pellet exosomes or TLVs. The

obtained pellets were washed once with large volume of PBS and resuspended for further analysis.

For quantification of exosome production, the membrane pellets isolated from 10 mL 24-h culture supernatant of normal cells or FITC-TCS-treated K562 cells were resuspended in 250 μL of PBS and then quantified by measuring the activity of acetylcholinesterase as described by Savina et al. (57). For TLV quantification, the vesicle solution obtained from the FITC-TCS-treated K562 cells was further analyzed by fluorescence spectrophotometer at 495-nm excitation and 515-nm emission.

Fluorescence microscopy

For intercellular targeting of exosomes, two groups of cells were treated with FITC-TCS or TRITC-TCS, respectively, for pulse 30 min and then chase 90 min. After extensive washing with cold PBS, equivalent amount of cells from different groups was mixed, co-incubated for 120 min and then fixed with 4% paraformaldehyde at 4°C.

All samples were mounted with 90% glycerol in PBS and visualized on a Nikon E800 microscope with fluorescence attachment using a Plan-Apochromat 100× 1.4 numerical aperture oil objective. Digital images were acquired with a SPOT RT cold charge-coupled device camera driven by the SPOT 3.5 software.

Laser scanning confocal microscopy

Roughly 10^5 JAR cells were grown to 60% confluency on 12-mm coverslips and incubated with TCS for 2 h at 4°C. Cells were washed extensively with ice-cold PBS for four times and chased for another 2 h in complete RPMI-1640 medium. Then, cells were fixed with 4% formaldehyde, permeated using 0.05% (w/v) saponin and incubated with appropriated primary and second antibodies. Coverslips were mounted in antifade solution (Roche) and examined using an LSM510 ZEISS laser scanning confocal microscopy.

RNAi analysis

Vector-based silencing of Tsg101 was achieved using small interfering RNA (siRNA) plasmid pBS/U6/T that was constructed by directly inserting complementary oligonucleotides containing Tsg101 target sequence (in boldface) (sense, 5′-**CCTCCAGTCTTCTCTCGTC**TTC AAGAGA**GACGAGA-GAAGACTGGAGG**TTTTTG-3′; antisense, 5′-AATT CAAAAA**CCTC-CAGTCTTCTCTCGTC**TCTCTTGAA**GACGAGAGAAGACTGGAGG**-3′) (58) into *Apa*I and *Eco*RI sites of pBS/U6 vector (a kind gift of Dr Y. Shi, Harvard University). Besides, a plasmid with insertion of a scrambled sequence (5′-GGGGCGAGGCAGC GGCACC-3′) (pBS/U6/NC) (59) was used as a negative control. To silence human nSMase2, we took advantage of the siRNA technique using the specific siRNA duplex targeting nSMase2 already proven to be efficient in silencing the enzyme in human cells (60). The scrambled siRNA (control) was obtained from GeneChem Company.

For electroporation, 1.4×10^7 K562 cells were mixed with 20 μg plasmid or 2 nmol siRNA in 0.7 mL cold PBS with 10 mM HEPES in 0.4-cm-gap cuvettes and treated with a BTX ECM 399 electroporator (BTX division of Genetronics Inc) at 300 V for 20–25 milliseconds. For Tsg101 RNAi analysis, the secretion of total exosomes or TLV was measured 72 h after transfection. For nSMase2 RNAi analysis, siRNA was delivered into K562 cells and repeated after 48 h, followed by another 24 h of incubation before carrying out the experiment. The efficient knockdown of Tsg101 was confirmed by western blotting and that of nSMase2 by reverse transcriptase–polymerase chain reaction because of lack of antibodies. The primers used were as follows: *nSMase2*, 5′-CTACAGCACAACCGAGTTTGTAAC-3′ (forward), 5′-TGGACGAAGCTTAAGAGGAGATAC-3′ (reverse); *β-actin*, 5′-ATTGGCAATGAGCGGTTCC-3′ (forward), 5′-GGTAGTTTCGTGGATGCCA-CA-3′ (reverse).

Cholesterol depletion and SMase treatment

For cyclodextrin treatment, exosomes or TLV isolated from 10 mL cell culture supernatant were resuspended in 950 μL PBS and then mixed with 50 μL of 100 mM MBCD and incubated at 37°C for 6 h. After cooling, samples were extracted with 1% Triton-X-100 (final concentration) on ice for 6 h and then centrifuged at 180 000 × ***g*** for 2 h. For SMase treatment, 1 mL exosome or TLV solution was incubated with 0.5 units SMase in PBS at 37°C for 6 h and then submitted to Triton extraction. For MBCD and SMase double treatment, 1 mL exosome or TLV solution was incubated with 0.5 units SMase and 10 mM MBCD in PBS at 37°C for 6 h before Triton extraction.

Immunoelectron microscopy

For ultrathin cell sections, JAR and K562 cells were treated with TCS or purified TLV for indicated periods and then fixed, treated with 1% OsO_4, gradually dehydrated by acetone and finally embedded in Epon-812. Ultrathin sections (<80 nm) were cut with a glass knife and immunogold labeled for TCS (5-nm gold particles), Tsg101 and flotillin2 (10-nm gold particles) as described previously (61).

For isolated TLVs, droplets of PBS with suspended membrane pellets obtained from 100 000 × ***g*** centrifugation were put on Formvar-coated electron microscope grids, fixed and immunolabeled.

Sucrose density gradient centrifugation

For characterization of secreted TCS, the 120 min chasing supernatant of K562 cells that were pulse treated with 0.2 μM TCS for 30 min was collected and centrifuged at 300 × ***g*** for 10 min, 800 × ***g*** twice for 15 min and 10 000 × ***g*** for 30 min to remove cell debris. The supernatant was filtered through a 0.22-μm filter, concentrated by Centriprep filtration and then floated on a 0.25–2.5 M continuous sucrose density gradient at 270 000 × ***g*** for 18 h as described previously (21).

For raft identification, the purified TLVs were permeated with 0.1% Triton-X-100 in PBS at room temperature for 30 min and then centrifuged at 100 000 × ***g*** for 2 h. The membrane pellets were resuspended in 1 mL cold 1% Triton-X-100 in 20 mM HEPES, 150 mM NaCl (pH 7.2 buffer), homogenized and incubated at 4°C overnight. Then, the homogenate was analyzed by a discrete gradient of 40, 30 and 5% sucrose at 270 000 × ***g*** for 18 h as described previously (62).

[^{3}H]Leucine incorporation assay

Aliquots of 5×10^4 cells were cultured in 1 mL of medium in 24-well plates (Falcon) in duplicates on the day before the experiment. Then, 70 ng of TCS, TLV containing 70 ng of TCS or the same amount of NE was added into wells and the cells were incubated for the indicated times. After incubation, the cells were washed with 20 mM HEPES (pH 7.2) buffer containing 0.14 M NaCl and then treated with 1 μCi of [^{3}H]leucine in 1 mL of leucine-free medium for 20 min. At the end of labeling, the medium was removed and 1 mL of 5% (w/v) trichloroacetic acid was added. After incubation for 10 min at room temperature, the trichloroacetic acid was sucked off and another 1 mL of trichloroacetic acid was added. After further 10-min incubation, the trichloroacetic acid was removed and the cells were solubilized in 200 μL of 0.1 M KOH. The dissolved cells were transferred to counting vials, 1 mL of Insta-Gel Plus (Perkin Elmer) was added to each vial and after swirling the vial on a Whirley mixer, the radioactivity was measured by liquid scintillation counting. The results are expressed as the percentage of the leucine incorporation in the untreated control cells. The incorporation in the controls varied between 6000 and 20 000 c.p.m. in three different experiments.

Cytotoxicity analysis

Cells were seeded in 96-well plates at 1×10^4 cells/well for JAR cells and K562 cells, 2×10^4 cells/well for Jurkat cells and 1.6×10^5 cells/well for NK92 cells. Then, free TCS, purified TLV or NE was added into the growth medium for incubation at 37°C for 48 h. The amount of TCS on TLV was determined by immunoblotting against anti-TCS antibody. The amount of TLV and NE were normalized by the TfR protein quantified using immunoblotting. Cells grown in normal medium without treatment were used as

controls. Survival of cells was detected by MTT reduction method, and the cell death ratio was calculated from the following equation:

$$\text{Cell death ratio} = 1 - (\text{OD550}_{\text{TCS or TLV}}/\text{OD550}_{\text{control}}).$$

Liposome preparation

Small unilamellar liposomes were prepared as follows: the lipid mixture with exosome-like composition (30), raft-like composition (PC:PE:cholesterol:sphingomyelin = 0.7:0.7:2.2:1, in molar ratio, plus 1% ganglioside in wt %) and only neutral phospholipids (PC:PE = 1:1, in molar ratio) were dried under a stream of nitrogen and vacuumized for at least 4 h to remove residual solvents. The lipid films were resuspended in pH 5.0 acetate buffer with 100 mM NaCl and then sonicated to near optical clarity using a Cole-Parmer ultrasonic homogenizer (model CP601) equipped with a cup horn accessory.

Acknowledgments

We thank Dr Y. Shi for kindly providing pBS/U6 vector; Dr Y. Shi, Y. Zhong and Y. Chen for extensive and fruitful discussion and W. L. Jiang for the help of electron microscopy. This research was supported by National Natural Science Foundation of China and National Basic Research Program of China (2004CB720005).

Supporting Information

Additional Supporting Information may be found in the online version of this article:

Figure S1: Cytotoxicity of TCS and FITC-TCS. JAR (A) and K562 (B) cells were incubated with indicated amounts of TCS or FITC-TCS for 48 h at 37°C. Cells grown in the absence of TCS and FITC-TCS were used as controls. The death ratio was measured using the MTT method as described in the *Materials and Methods*. The bars indicate the mean ± SEM of three independent experiments.

Figure S2: Transport dynamic of internalized TCS in JAR (A–E) and K562 cells (F–J). Cells were treated with FITC-TCS at 37°C for 10 min (A), 30 min (B and F) or pulse treated for 30 min and then chase incubated in TCS-free medium for additional 30–120 min (C–E and G–J). Insets show magnified TCS-targeted organelles. Fluorescence images (FLU) and merged images with differential interference contrast photos (Merge) are shown. Scale bar, 3 μm.

Figure S3: A) Vector-based silencing of Tsg101 in K562 cells. K562 cells were electroporated with pBS/U6/T (siRNA of Tsg101) or pBS/U6/NC (control) as described in *Materials and Methods*. The expression of Tsg101 and β-actin in RNAi cells and in control cells was detected by western blotting after 72–96 h of transfection. B) siRNA induced silencing of human nSMase2 in K562 cells. Cells were electroporated with nSMase2 siRNA or scrambled siRNA (control) as described in *Materials and Methods*. The efficient knockdown was monitored by measuring the levels of nSMase2 by reverse transcriptase–polymerase chain reaction after 72–96 h of the first transfection.

Figure S4: Lipid monolayer analysis of the interaction of TCS with lipid membrane containing different composition. Lipid monolayers with a raft-like composition or with PC/PE were prepared as described in Materials and Methods. Acetate buffer (50 mM acetate, 100 mM NaCl, pH 5.0) was used as the subphase, and the final concentration of TCS was 200 nM. Left, the π-t curves of TCS penetration at an initial surface pressure (πi) of 13 mN/m. Right, the Δπ-πi curves of TCS insertion into the raft monolayer (▲) and the PC/PE monolayer (●). πc shows the critical insertion pressure of TCS for the indicated lipid monolayer.

Figure S5: Fluorescence quenching analyses on the interaction of TCS with lipid membrane containing different composition. One micromolar TCS was incubated with 50 μM (+), 100 μM (▲) or 150 μM (■) spin-labeled (12-DOXYL PC) liposomes containing either a raft-like composition (left) or PC/PE (right) at 37°C and pH 5.0 acetate buffer for at least 30 min. Then, the tryptophan fluorescence of TCS was determined at an excitation wavelength of 280 nm. The fluorescence of TCS incubated with 50–150 μM liposomes without spin labeling defined as 100% (●). The background spectra of the liposomes were subtracted.

Figure S6: FITC-labeled TLVs interact with the Jurkat cell (A) or the NK92 cell (B). Cells were incubated with purified FITC-labeled TLV for 30 min. Then, cells were washed extensively and fixed with 4% paraformaldehyde at 4°C. Differential interference contrast photos (DIC), fluorescence images (FLU) and merged images (Merge) are shown. Scale bar, 5 μm.

Figure S7: TCS stimulates exosome production in K562 cells. Exosomes were isolated from the culture supernatant of K562 cells growing without (control) or with TCS at indicated concentrations and then quantified by measuring acetylcholinesterase activity or by densitometric analysis of the immunoblotting bands of flotillin2 (lower panel).

Please note: Wiley-Blackwell are not responsible for the content or functionality of any supporting materials supplied by the authors. Any queries (other than missing material) should be directed to the corresponding author for the article.

References

1. Sandvig K, van Deurs B. Membrane traffic exploited by protein toxins. Annu Rev Cell Dev Biol 2002;18:1–24.
2. Collier RJ. Understanding the mode of action of diphtheria toxin: a perspective on progress during the 20th century. Toxicon 2001;39: 1793–1803.
3. Sandvig K, van Deurs B. Entry of ricin and Shiga toxin into cells: molecular mechanisms and medical perspectives. Embo J 2000;19: 5943–5950.
4. Zhang XJ, Wang JH. Homology of trichosanthin and ricin A chain. Nature 1986;321:477–478.
5. Maraganore JM, Joseph M, Bailey MC. Purification and characterization of trichosanthin. Homology to the ricin A chain and implications as to mechanism of abortifacient activity. J Biol Chem 1987;262: 11628–11633.
6. Zhang JS, Liu WY. The mechanism of action of trichosanthin on eukaryotic ribosomes – RNA N-glycosidase activity of the cytotoxin. Nucleic Acids Res 1992;20:1271–1275.
7. Tsao SW, Yan KT, Yeung HW. Selective killing of choriocarcinoma cells in vitro by trichosanthin, a plant protein purified from root tubers of the Chinese medicinal herb *Trichosanthes kirilowii*. Toxicon 1986;24: 831–840.
8. Ng TB, Chan WY, Yeung HW. Proteins with abortifacient, ribosome inactivating, immunomodulatory, antitumor and anti-AIDS activities from Cucurbitaceae plants. Gen Pharmacol 1992;23:579–590.
9. Shaw PC, Chan WL, Yeung HW, Ng TB. Minireview: trichosanthin – a protein with multiple pharmacological properties. Life Sci 1994;55: 253–262.

10. McGrath MS, Hwang KM, Caldwell SE, Gaston I, Luk KC, Wu P, Ng VL, Crowe S, Daniels J, Marsh J, Deinhart T, Lekas PV, Vennari JC, Yeung HW, Lifson JD. GLQ223: an inhibitor of human immunodeficiency virus replication in acutely and chronically infected cells of lymphocyte and mononuclear phagocyte lineage. Proc Natl Acad Sci U S A 1989;86: 2844–2848.
11. Byers VS, Levin AS, Waites LA, Starrett BA, Mayer RA, Clegg JA, Price MR, Robins RA, Delaney M, Baldwin RW. A phase I/II study of trichosanthin treatment of HIV disease. Aids 1990;4:1189–1196.
12. Chan WL, Shaw PC, Tam SC, Jacobsen C, Gliemann J, Nielsen MS. Trichosanthin interacts with and enters cells via LDL receptor family members. Biochem Biophys Res Commun 2000;270:453–457.
13. Chan WY, Huang H, Tam SC. Receptor-mediated endocytosis of trichosanthin in choriocarcinoma cells. Toxicology 2003;186:191–203.
14. van Niel G, Porto-Carreiro I, Simoes S, Raposo G. Exosomes: a common pathway for a specialized function. J Biochem (Tokyo) 2006;140:13–21.
15. Thery C, Boussac M, Veron P, Ricciardi-Castagnoli P, Raposo G, Garin J, Amigorena S. Proteomic analysis of dendritic cell-derived exosomes: a secreted subcellular compartment distinct from apoptotic vesicles. J Immunol 2001;166:7309–7318.
16. de Gassart A, Geminard C, Fevrier B, Raposo G, Vidal M. Lipid raft-associated protein sorting in exosomes. Blood 2003;102:4336–4344.
17. Taylor DD, Gercel-Taylor C. Tumour-derived exosomes and their role in cancer-associated T-cell signalling defects. Br J Cancer 2005;92: 305–311.
18. Fevrier B, Vilette D, Archer F, Loew D, Faigle W, Vidal M, Laude H, Raposo G. Cells release prions in association with exosomes. Proc Natl Acad Sci U S A 2004;101:9683–9688.
19. Stoorvogel W, Kleijmeer MJ, Geuze HJ, Raposo G. The biogenesis and functions of exosomes. Traffic 2002;3:321–330.
20. Gruenberg J. The endocytic pathway: a mosaic of domains. Nat Rev Mol Cell Biol 2001;2:721–730.
21. Raposo G, Nijman HW, Stoorvogel W, Liejendekker R, Harding CV, Melief CJ, Geuze HJ. B lymphocytes secrete antigen-presenting vesicles. J Exp Med 1996;183:1161–1172.
22. Wolfers J, Lozier A, Raposo G, Regnault A, Thery C, Masurier C, Flament C, Pouzieux S, Faure F, Tursz T, Angevin E, Amigorena S, Zitvogel L. Tumor-derived exosomes are a source of shared tumor rejection antigens for CTL cross-priming. Nat Med 2001;7:297–303.
23. Savina A, Furlan M, Vidal M, Colombo MI. Exosome release is regulated by a calcium-dependent mechanism in K562 cells. J Biol Chem 2003;278:20083–20090.
24. Savina A, Fader CM, Damiani MT, Colombo MI. Rab11 promotes docking and fusion of multivesicular bodies in a calcium-dependent manner. Traffic 2005;6:131–143.
25. Fernandez-Borja M, Wubbolts R, Calafat J, Janssen H, Divecha N, Dusseljee S, Neefjes J. Multivesicular body morphogenesis requires phosphatidyl-inositol 3-kinase activity. Curr Biol 1999;9:55–58.
26. Clayton A, Court J, Navabi H, Adams M, Mason MD, Hobot JA, Newman GR, Jasani B. Analysis of antigen presenting cell derived exosomes, based on immuno-magnetic isolation and flow cytometry. J Immunol Methods 2001;247:163–174.
27. Raiborg C, Rusten TE, Stenmark H. Protein sorting into multivesicular endosomes. Curr Opin Cell Biol 2003;15:446–455.
28. Trajkovic K, Hsu C, Chiantia S, Rajendran L, Wenzel D, Wieland F, Schwille P, Brugger B, Simons M. Ceramide triggers budding of exosome vesicles into multivesicular endosomes. Science 2008;319:1244–1247.
29. Wubbolts R, Leckie RS, Veenhuizen PT, Schwarzmann G, Mobius W, Hoernschemeyer J, Slot JW, Geuze HJ, Stoorvogel W. Proteomic and biochemical analyses of human B cell-derived exosomes. Potential implications for their function and multivesicular body formation. J Biol Chem 2003;278:10963–10972.
30. Laulagnier K, Motta C, Hamdi S, Roy S, Fauvelle F, Pageaux JF, Kobayashi T, Salles JP, Perret B, Bonnerot C, Record M. Mast cell and dendritic cell-derived exosomes display a specific lipid composition and an unusual membrane organization. Biochem J 2004;380:161–171.
31. Mobius W, van Donselaar E, Ohno-Iwashita Y, Shimada Y, Heijnen HF, Slot JW, Geuze HJ. Recycling compartments and the internal vesicles of multivesicular bodies harbor most of the cholesterol found in the endocytic pathway. Traffic 2003;4:222–231.
32. Fevrier B, Raposo G. Exosomes: endosomal-derived vesicles shipping extracellular messages. Curr Opin Cell Biol 2004;16:415–421.
33. Thery C, Zitvogel L, Amigorena S. Exosomes: composition, biogenesis and function. Nat Rev Immunol 2002;2:569–579.
34. Lancaster GI, Febbraio MA. Exosome-dependent trafficking of HSP70: a novel secretory pathway for cellular stress proteins. J Biol Chem 2005;280:23349–23355.
35. Gupta S, Knowlton AA. HSP60 trafficking in adult cardiac myocytes: role of the exosomal pathway. Am J Physiol Heart Circ Physiol 2007; 292:H3052–H3056.
36. Johnstone RM. Exosomes biological significance: a concise review. Blood Cells Mol Dis 2006;36:315–321.
37. Muntasell A, Berger AC, Roche PA. T cell-induced secretion of MHC class II-peptide complexes on B cell exosomes. EMBO J 2007;26:4263–4272.
38. Razi M, Futter CE. Distinct roles for Tsg101 and Hrs in multivesicular body formation and inward vesiculation. Mol Biol Cell 2006;17:3469–3483.
39. Marsh M, van Meer G. Cell biology. No ESCRTs for exosomes. Science 2008;319:1191–1192.
40. Laulagnier K, Vincent-Schneider H, Hamdi S, Subra C, Lankar D, Record M. Characterization of exosome subpopulations from RBL-2H3 cells using fluorescent lipids. Blood Cells Mol Dis 2005;35:116–121.
41. Quah BJ, O'Neill HC. The immunogenicity of dendritic cell-derived exosomes. Blood Cells Mol Dis 2005;35:94–110.
42. Subra C, Laulagnier K, Perret B, Record M. Exosome lipidomics unravels lipid sorting at the level of multivesicular bodies. Biochimie 2007;89:205–212.
43. Calzolari A, Raggi C, Deaglio S, Sposi NM, Stafsnes M, Fecchi K, Parolini I, Malavasi F, Peschle C, Sargiacomo M, Testa U. TfR2 localizes in lipid raft domains and is released in exosomes to activate signal transduction along the MAPK pathway. J Cell Sci 2006;119:4486–4498.
44. Abrami L, Lindsay M, Parton RG, Leppla SH, van der Goot FG. Membrane insertion of anthrax protective antigen and cytoplasmic delivery of lethal factor occur at different stages of the endocytic pathway. J Cell Biol 2004;166:645–651.
45. Milne JC, Furlong D, Hanna PC, Wall JS, Collier RJ. Anthrax protective antigen forms oligomers during intoxication of mammalian cells. J Biol Chem 1994;269:20607–20612.
46. Mack M, Kleinschmidt A, Bruhl H, Klier C, Nelson PJ, Cihak J, Plachy J, Stangassinger M, Erfle V, Schlondorff D. Transfer of the chemokine receptor CCR5 between cells by membrane-derived microparticles: a mechanism for cellular human immunodeficiency virus 1 infection. Nat Med 2000;6:769–775.
47. Greco V, Hannus M, Eaton S. Argosomes: a potential vehicle for the spread of morphogens through epithelia. Cell 2001;106:633–645.
48. Bedford P, Garner K, Knight SC. MHC class II molecules transferred between allogeneic dendritic cells stimulate primary mixed leukocyte reactions. Int Immunol 1999;11:1739–1744.
49. Valadi H, Ekstrom K, Bossios A, Sjostrand M, Lee JJ, Lotvall JO. Exosome-mediated transfer of mRNAs and microRNAs is a novel mechanism of genetic exchange between cells. Nat Cell Biol 2007;9:654–659.
50. White IJ, Bailey LM, Aghakhani MR, Moss SE, Futter CE. EGF stimulates annexin 1-dependent inward vesiculation in a multivesicular endosome subpopulation. EMBO J 2006;25:1–12.
51. Temchura VV, Tenbusch M, Nchinda G, Nabi G, Tippler B, Zelenyuk M, Wildner O, Uberla K, Kuate S. Enhancement of immunostimulatory

properties of exosomal vaccines by incorporation of fusion-competent G protein of vesicular stomatitis virus. Vaccine 2008;26:3662–3672.
52. Zhou H, Yuen PS, Pisitkun T, Gonzales PA, Yasuda H, Dear JW, Gross P, Knepper MA, Star RA. Collection, storage, preservation, and normalization of human urinary exosomes for biomarker discovery. Kidney Int 2006;69:1471–1476.
53. Andre F, Schartz NE, Movassagh M, Flament C, Pautier P, Morice P, Pomel C, Lhomme C, Escudier B, Le Chevalier T, Tursz T, Amigorena S, Raposo G, Angevin E, Zitvogel L. Malignant effusions and immunogenic tumour-derived exosomes. Lancet 2002;360:295–305.
54. Caby MP, Lankar D, Vincendeau-Scherrer C, Raposo G, Bonnerot C. Exosomal-like vesicles are present in human blood plasma. Int Immunol 2005;17:879–887.
55. Leung KN, Yeung HW, Leung SO. The immunomodulatory and antitumor activities of trichosanthin-an abortifacient protein isolated from tian-hua-fen (*Trichosanthes kirilowii*). Asian Pac J Allergy Immunol 1986;4:111–120.
56. Xia XF, Sui SF. The membrane insertion of trichosanthin is membrane-surface-pH dependent. Biochem J 2000;3:835–841.
57. Savina A, Vidal M, Colombo MI. The exosome pathway in K562 cells is regulated by Rab11. J Cell Sci 2002;115:2505–2515.
58. Garrus JE, von Schwedler UK, Pornillos OW, Morham SG, Zavitz KH, Wang HE, Wettstein DA, Stray KM, Cote M, Rich RL, Myszka DG, Sundquist WI. Tsg101 and the vacuolar protein sorting pathway are essential for HIV-1 budding. Cell 2001;107:55–65.
59. Bache KG, Raiborg C, Mehlum A, Stenmark H. STAM and Hrs are subunits of a multivalent ubiquitin-binding complex on early endosomes. J Biol Chem 2003;278:12513–12521.
60. Marchesini N, Osta W, Bielawski J, Luberto C, Obeid LM, Hannun YA. Role for mammalian neutral sphingomyelinase 2 in confluence-induced growth arrest of MCF7 cells. J Biol Chem 2004;279:25101–25111.
61. Slot JW, Geuze HJ, Gigengack S, Lienhard GE, James DE. Immunolocalization of the insulin regulatable glucose transporter in brown adipose tissue of the rat. J Cell Biol 1991;113:123–135.
62. Chamberlain LH, Burgoyne RD, Gould GW. SNARE proteins are highly enriched in lipid rafts in PC12 cells: implications for the spatial control of exocytosis. Proc Natl Acad Sci U S A 2001;98:5619–5624.